Optical Materials 47 (2015) 445–452

Contents lists available at ScienceDirect

Optical Materials

journal homepage: www.elsevier.com/locate/optmat

Experimental and theoretical investigation of the electronic structure and optical properties of $TlHgCl_3$ single crystal

A.H. Reshak [a,b,*], I.V. Kityk [c], Z.A. Alahmed [d], S. Levkovets [e], A.O. Fedorchuk [f], G. Myronchuk [g], K.J. Plucinski [h], H. Kamarudin [b], S. Auluck [i,j]

[a] New Technologies – Research Centre, University of West Bohemia, Univerzitni 8, 306 14 Pilsen, Czech Republic
[b] Center of Excellence Geopolymer and Green Technology, School of Material Engineering, University Malaysia Perlis, 01007 Kangar, Perlis, Malaysia
[c] Faculty of Electrical Engineering, Czestochowa University Technology, Armii Krajowej 17, PL-42-201 Czestochowa, Poland
[d] Department of Physics and Astronomy, King Saud University, Riyadh 11451, Saudi Arabia
[e] Department of Inorganic and Physical Chemistry, Eastern European National University, Voli 13, Lutsk 43025, Ukraine
[f] Department of Inorganic and Organic Chemistry, Lviv National University of Veterinary Medicine and Biotechnologies, Pekarska St., 50, 79010 Lviv, Ukraine
[g] Department of Solid State Physics, Eastern European National University, Voli 13, Lutsk 43025, Ukraine
[h] Electronic Department, Warsaw Military University, Kaliskiego 2, 00-908 Warsaw, Poland
[i] Council of Scientific and Industrial Research – National Physical Laboratory Dr. K S Krishnan Marg, New Delhi 110012, India
[j] Department of Physics, Indian Institute of Technology Delhi, Hauz Khas, New Delhi 110016, India

ARTICLE INFO

Article history:
Received 14 May 2015
Received in revised form 6 June 2015
Accepted 8 June 2015
Available online 15 June 2015

Keywords:
$TlHgCl_3$
Crystallographic data
Linear optical properties
Electronic charge density

ABSTRACT

We have synthesized single crystals of $TlHgCl_3$, which posses an orthorhombic symmetry, space group *Pnma*, with lattice constants $a = 9.1601(4)$ Å, $b = 4.3548(2)$ Å and $c = 14.0396(5)$ Å. The measurements of the optical absorption of $TlHgCl_3$ are performed on parallel-plate samples with polished optical quality surfaces of $d = 0.03$ mm. The band gap is estimated to be 2.74 eV from the position of fundamental absorption edge at $\alpha = 200\ cm^{-1}$. We have used our measured crystallographic data of $TlHgCl_3$ as input data for calculating the electronic band structure, density of states, electronic charge density and the optical properties. The all-electron full potential linearized augmented plane wave plus local orbital (FP-L(APW + lo)) method is used. Calculations are performed with three types of exchange correlations; local density approximation (LDA), general gradient approximation (PBE-GGA) and the recently modified Becke-Johnson potential (mBJ). The PBE-GGA is used to optimize the atomic positions by minimization of the forces (1 mRy/au) acting on the atoms. The obtained values of the band gap from various exchange correlations are 2.39 eV (LDA), 2.55 eV (PBE-GGA) and 2.69 eV (mBJ). It is clear that mBJ succeeded by a large amount in bringing the calculated energy gap closer to the experimental one. The calculated electronic band structure exhibits that the conduction band minimum and the valence band maximum are located at Z point of the BZ, resulting in a direct band gap. The calculated density of states provides information about the hybridization between the states and the bonding nature. The electronic charge density show that Hg and Cl atoms form partial ionic/covalent bonding between Cl–Hg–Cl. Furthermore, for a deep insight into the electronic structure we have investigated the optical properties.

1. Introduction

$ABCl_3$ crystals belong to a class of generic compounds ABX_3, where A is a monovalent cation, B a divalent cation and X is a halogen. Various crystals of this series suggest a relation between electric and magnetic ordering, ferroelectric/anti-ferroelectricity, ferro- and anti-ferromagnetism. The presence of structural and magnetic transitions is of interest to professionals involved in the problem of phase transitions. The simple crystal structure has allowed research workers to model phase transformations. Furthermore the $ABCl_3$ compounds are of significant interest due to the possibility of using them in acousto-optical control systems with laser beams [1–4]. A recent work presented the possibility of using them as piezo-optical sensors [4]. Also it was reported to have a possible application as scintillators [5]. Moreover, due to

* Corresponding author at: New Technologies – Research Centre, University of West Bohemia, Univerzitni 8, 306 14 Pilsen, Czech Republic.
E-mail addresses: maalidph@yahoo.co.uk, maalidph@yahoo.com (A.H. Reshak), iwank74@gmail.com (I.V. Kityk), zalahmed@KSU.EDU.SA (Z.A. Alahmed), ya.hhhggg@yandex.ua (S. Levkovets), ft@ua.fm (A.O. Fedorchuk), g_muronchuk@ukr.net (G. Myronchuk), kpluc2006@wp.pl (K.J. Plucinski), sauluck@gmail.com (S. Auluck).

http://dx.doi.org/10.1016/j.optmat.2015.06.018
0925-3467/

Fig. 1. $TlHgCl_3$ single crystal.

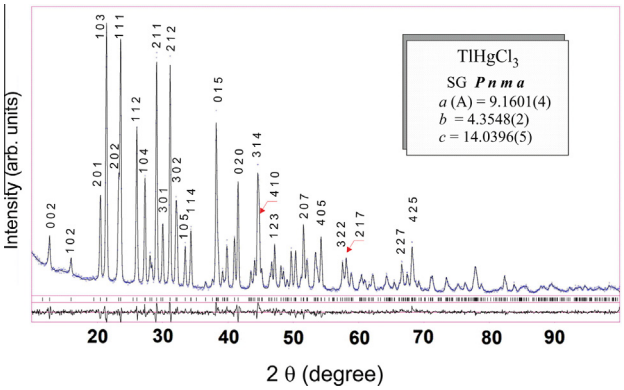

Fig. 2. Experimental and theoretical diffraction patterns of the $TlHgCl_3$ compound and their difference.

the large optical anisotropy these crystals may be uses as materials for formation of the optical polarisers, filters and beam splitters in the spectral range from visible up to infrared. Therefore, studies of their electronic structure and related optical dispersions are very interesting. Another promising application of such compounds is in the area of solar cells similar to the ternary halide perovskites [6–9]. The presence of heavy cations like Tl and Hg leads to suppress of the phonon subsystem during the photo-carrier transport. Thus the studies of their band energy dispersions, which define the carrier mobility, are very important. It is very crucial to know the anisotropy of the carrier effective masses and the partial contributions of the different energy terms defining the principal properties.

It is necessary to emphasize that the $ABCl_3$ crystals posses a large number of structural modifications. Generally, the structure of these compounds can be represented as octahedra formed by BCl_6, related corners or edges [10]. Earlier the formation of four different structural types in the system $TlX–HgX_2$ (X = Cl, Br, I) has been reported [11]. The effect of composition and type of chemical connection on the optical properties $ABCl_3$ has been studied [12]. It has been suggested that $TlHgCl_3$ is isotype of NH_4CdCl_3 [13,14], although it is less toxic. In order to clarify the origin of the optical and electronic features of $TlHgCl_3$ crystals, in the present work we perform density functional theory (DFT) band structure calculation which allows us to obtain information concerning the density of states, charge density distribution and optical properties.

Due to a lack of structural information of $TlHgCl_3$, we have determined the structural parameters of $TlHgCl_3$ single crystals experimentally. Since there is no detailed information about the electronic structure of $TlHgCl_3$, further insight into the electronic structure can be obtained from the optical properties. We would like to mention that we are not aware of calculations or experimental data for the electronic structure and linear optical susceptibilities for $TlHgCl_3$. Therefore we thought it worthwhile to synthesize single crystals of $TlHgCl_3$, to measure and calculate some specific features of the electronic structure and the optical properties. Calculations are performed using full potential method using three types of exchange correlation potentials in order to ascertain the effect of exchange correlation on the electronic structure and the optical properties. First-principles calculations have provided a strong and useful tool to predict the crystal structure and calculate its properties related to the electron configuration of a material before its synthesis [15–18].

2. Results and discussions

2.1. Experimental work

2.1.1. Single crystal preparation of $TlHgCl_3$

Binary chlorides are used for the production of $TlHgCl_3$ crystals. TlCl is obtained from the reaction of the respective nitrate with hydrochloric acid. It is then refined by the oriented crystallization using the vertical version of Bridgman–Stockbarger method and 30-fold zone melting. Commercial mercury chloride is additionally purified by vacuum distillation. According to $TlCl–HgCl_2$ phase diagram $TlHgCl_3$ melts congruently at 497 K [19]. Therefore we used the method of directed crystallization in a two-zone furnace for the production of its crystals. The following growth conditions were applied: growth zone/annealing zone temperature = 553 K/453 K, temperature gradient at the solid–melt interface 0.7 K/cm, growth rate of 1.2 cm/day. The $TlHgCl_3$ single crystals are illustrated in Fig. 1.

2.1.2. Crystallographic data of $TlHgCl_3$

The diffraction pattern of the sample with $TlHgCl_3$ composition is recorded using a DRON 4-13 diffractometer with Cu Kα radiation and a Ni filter is indexed in the assumption of the orthorhombic cell with the periods $a = 9.1601(4)$ Å, $b = 4.3548(2)$ Å, $c = 14.0396(5)$ Å. The best fit for the reflection positions and intensity of our diffraction pattern and those of the known $A^IB^{II}H_3$ compounds is obtained for $TlCdCl_3$ [20]. Therefore the data for $TlCdCl_3$ are used as a starting model. The refinement of the crystallographic

Table 1
Crystallographicx data for $TlHgCl_3$ (SG *Pnma* (62); $a = 9.1601(4)$ Å, $b = 4.3548(2)$ Å, $c = 14.0396(5)$ Å; cell volume (Å^3) = 560.05(6); calculated density (g/cm^3) = 6.0636(7)). In additional we present the optimized atomic position after we minimized of the forces acting on the atoms to be less than 1 mRy/a.u. For more details about the crystal structure of $TlHgCl_3$ we refer the readers to the attached cif file.

Element	Wyckoff	*x* exp.	*x* opt.	*y* exp.	*y* opt.	*z* exp.	*z* opt.	*B*
Hg	4*c*	0.1754(3)	0.1744	1/4	1/4	0.4537(2)	0.4526	1.37(8)
Tl	4*c*	0.4493(3)	0.4489	1/4	1/4	0.6692(2)	0.6688	1.69(8)
Cl1	4*c*	0.2723(14)	0.2739	1/4	1/4	0.2936(9)	0.2928	1.8(6)
Cl2	4*c*	0.1552(14)	0.1548	1/4	1/4	0.0156(9)	0.0154	0.9(5)
Cl3	4*c*	0.0419(14)	0.0427	1/4	1/4	0.6024(8)	0.6042	0.8(5)

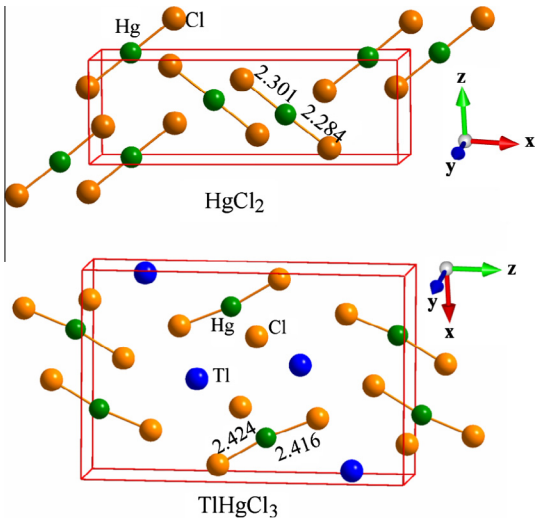

Fig. 3. The location of "$HgCl_2$" fragments in the structure of $HgCl_2$ and $TlHgCl_3$ compounds.

parameters is performed by Rietveld method. The refined and standardized crystallography data for $TlHgCl_3$ within fit factors $R_{(I/P)}$ = 0.0440/0.0997 are presented in Table 1 and Fig. 2. In the $TlHgCl_3$ the Hg atoms occupy the positions of Cd atoms in the $TlCdCl_3$ structure (Fig. 3) and may be typical for the Tl containing cation [21], while the correctness of this choice is confirmed by the analogous closest surrounding of Hg atoms (in "$HgCl_2$" fragments in the structure of $HgCl_2$ [22] and $TlHgCl_3$). The coordination surrounding of the atoms of metallic components and inter-atomic distances in the $TlHgCl_3$ structure are represented in Fig. 4. For more details about the crystal structure we refer to the attached cif file which contains all the information about $TlHgCl_3$ structure.

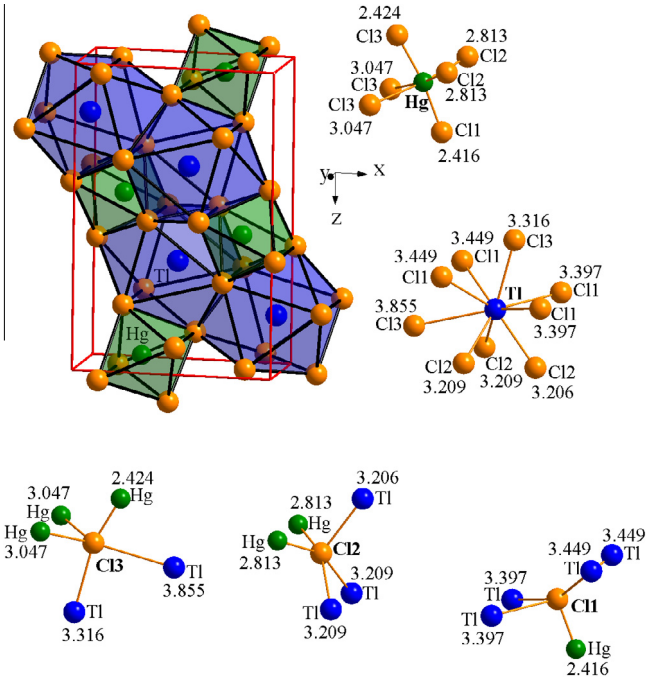

Fig. 4. Coordination surrounding and inter-atomic distances in the $TlHgCl_3$ structure.

2.1.3. Optical absorption of $TlHgCl_3$

The measurements are performed on parallel-plate samples with polished optical quality surfaces of d = 0.03 mm. The band gap is estimated by the position of fundamental absorption edge at $\alpha = 200\ cm^{-1}$ is about 2.74 eV. The spectral region below the intrinsic absorption edge featured exponential dependence of the absorption coefficient (α) on the photon energy (E):

$$\alpha \sim \exp[-(E_g - E)/\Delta] \quad (1)$$

where E_g is the energy band gap, E is the photon energy, Δ is the specific energy that reflects the slope of the absorption tail and is determined by the degree of the disorder of the crystal lattice. Its value is determined (Fig. 5) from the inverse slope of the line ln $\alpha = f(E)$:

$$\Delta = dE/d \ln \alpha \quad (2)$$

Such dependence is caused by the non-uniformities of electrostatic and deformation potentials which lead to the appearance of tails of the state density within the band gap of a semi-conductor [23]. The value of the specific energy Δ that is determined from the experimental dependence is 0.15 eV.

2.2. Theoretical work

2.2.1. Details of calculations

$TlHgCl_3$ crystallizes in a orthorhombic structure, space group *Pnma*, with lattice constants a = 9.1601(4) Å, b = 4.3548(2) Å and c = 14.0396(5) Å. The crystal structure of $TlHgCl_3$ is illustrated in Figs. 3 and 4. The full potential linear augmented plane wave plus local orbital (FP-L(APW + lo)) method in a scalar relativistic version as embodied in the WIEN2k code [24] is used for our calculations. This is an implementation of the DFT with different possible approximations for the exchange–correlation (XC) potential. Exchange and correlation potentials are described by LDA [25] and PBE-GGA [26], which is based on exchange–correlation energy optimization to calculate the total energy. In addition, we have used the recently modified Becke-Johnson potential (mBJ) [27] which optimizes the corresponding potential for electronic band structure calculations. The mBJ, a modified Becke-Johnson potential, allows the calculation of band gaps with accuracy similar to the very expensive GW calculations [27]. It is a local approximation to an atomic "exact-exchange" potential and a screening term.

Using PBE-GGA we have optimized the atomic positions by minimization of the forces acting on the atoms. The structure is fully relaxed until the forces on the atoms are less than 1 mRy/a.u. The optimized atomic positions along with those obtained from XRD are listed in Table 1. Once the forces are minimized in this construction one can then find the self-consistent density at these positions by turning off the relaxations and driving the system to self-consistency. From the obtained relaxed geometry the electronic structure and the chemical bonding can be determined and various spectroscopic features can be simulated and compared with experimental data. The Kohn–Sham equations are solved using a basis of linear APW's + lo. The potential and charge density in the muffin-tin (MT) spheres are expanded in spherical harmonics with l_{max} = 8 and nonspherical components up to l_{max} = 6. In the interstitial region the potential and the charge density are represented by Fourier series. Self-consistency is obtained using 300 $\vec{k}$ points in the irreducible Brillouin zone (IBZ). We have calculated the linear optical properties using 500 $\vec{k}$ points in the IBZ. The self-consistent calculations are converged since the total energy of the system is stable within 0.00001 Ry.

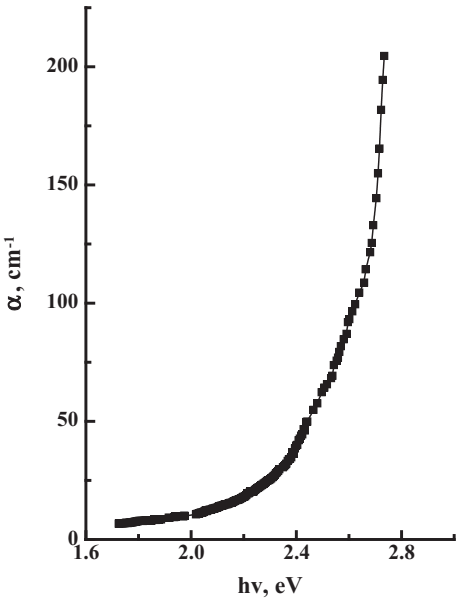

Fig. 5. Frequency dependence of the absorption coefficient in $TlHgCl_3$ single crystals at 292 K. We fit this measured absorption coefficient to the calculated one in Fig. 9(d) and (e).

2.2.2. Electronic band structure and density of states

The electronic band structure of $TlHgCl_3$ as shown in Fig. 6 is calculated using three types of exchange–correlation potentials in order to overcome the underestimation of the energy gap caused by LDA and GGA [28]. The calculated electronic band structure shows that the conduction band minimum (CBM) and the valence band maximum (VBM) are located at Z point of the Brillouin Zone (BZ), resulting in a direct band gap. We have obtained a gap of about 2.39 eV using LDA, 2.55 eV (PBE-GGA) and 2.69 eV (mBJ). It is clear that mBJ brings the calculated gap very close to our measured one (2.74 eV) obtained from the optical absorption measurement (Fig. 5). We should emphasize that the Fermi level (E_F) is located at zero eV and the VBM is set to be at E_F. One can see that the using different exchange–correlation potential leads to shift the CBM towards higher energies with respect to E_F resulting in increasing the energy gap as we go from LDA → PBE-GGA → mBJ to match the experimental gap.

To provide a deep insight into the electronic structure of $TlHgCl_3$ we have calculated the total and partial density of states (TDOS and PDOS). Fig. 7(a) illustrates the TDOS using the three exchange correlations mentioned above. The TDOS reiterates our previous finding that the CBM shift towards higher energies when one move from LDA → PBE-GGA → mBJ keeping the VBM situated at E_F. Since mBJ yielded an energy band gap close to the experimental one, therefore, we will present the results using mBJ only. The PDOS helps to identify the angular momentum character of the various structures. Fig. 7(b) shows that Tl-d states have only one structure which is located at −9.0 eV. Fig. 7((c)–(e)) illustrates that the structures in the energy region extended from −10.0 eV up to E_F is formed by Tl-s/p, Hg-s/p/d/f, and Cl-s/p states, with strong hybridization between Hg-s/p and Tl-p states and also between Hg-s and Cl-s states. The strong hybridization may lead to covalent bonding. The energy region extended between the CBM and above is mainly an admixture of Hg-s/p/f, Cl-s/p and Tl-s/p/f states with a weak hybridization between Cl-s and Hg-f and Tl-f states.

Now let us turn our attention to discus the nature of bonding among the atoms of $TlHgCl_3$. This can be explained using the map of electronic charge density distribution. The transfer of charge between anion and cation can be utilized to explain the ionic character of $TlHgCl_3$ whereas sharing the charge between anion and cation is related to the covalent character. Fig. 8(a) shows the electronic charge density distribution in the crystallographic plane (1 0 1) which represent the three types of atoms. This plot suggests that both of Hg and Cl atoms form partial ionic/-covalent bonding between Cl–Hg–Cl atoms according to the electronegativity difference between Hg (2.0) and Cl (3.16). It is clear that the electronic charge is concentrated around these atoms as indicated by the blue color. Also one can see that Tl atom forms an ionic bonding and the Cl atom which is far from Hg atom also forms an ionic bond. To investigate the anisotropy nature of bonding in $TlHgCl_3$ we have plotted the electronic charge density distribution in the crystallographic plane (−1 0 1) which also represent the three types of atoms and confirms that there exists partial ionic/covalent bonding between Cl–Hg–Cl (Fig. 8(b)). The

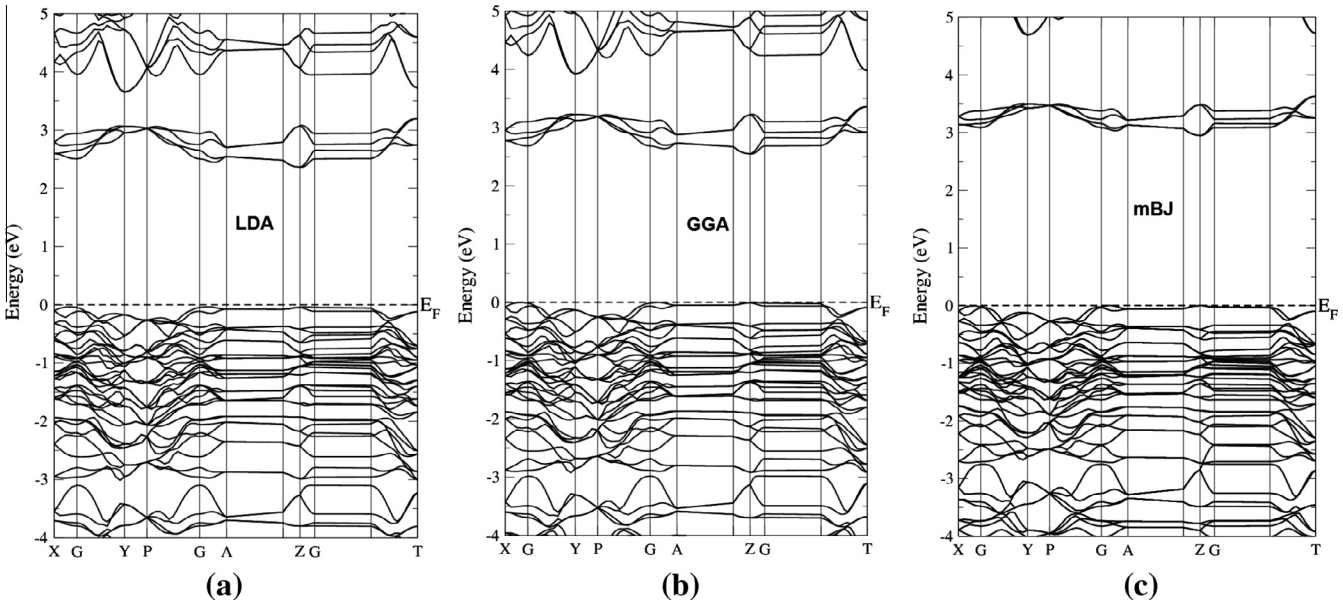

Fig. 6. Calculated electronic band structure: (a) CA-LDA; (b) PBE-GGA; and (c) mBJ.

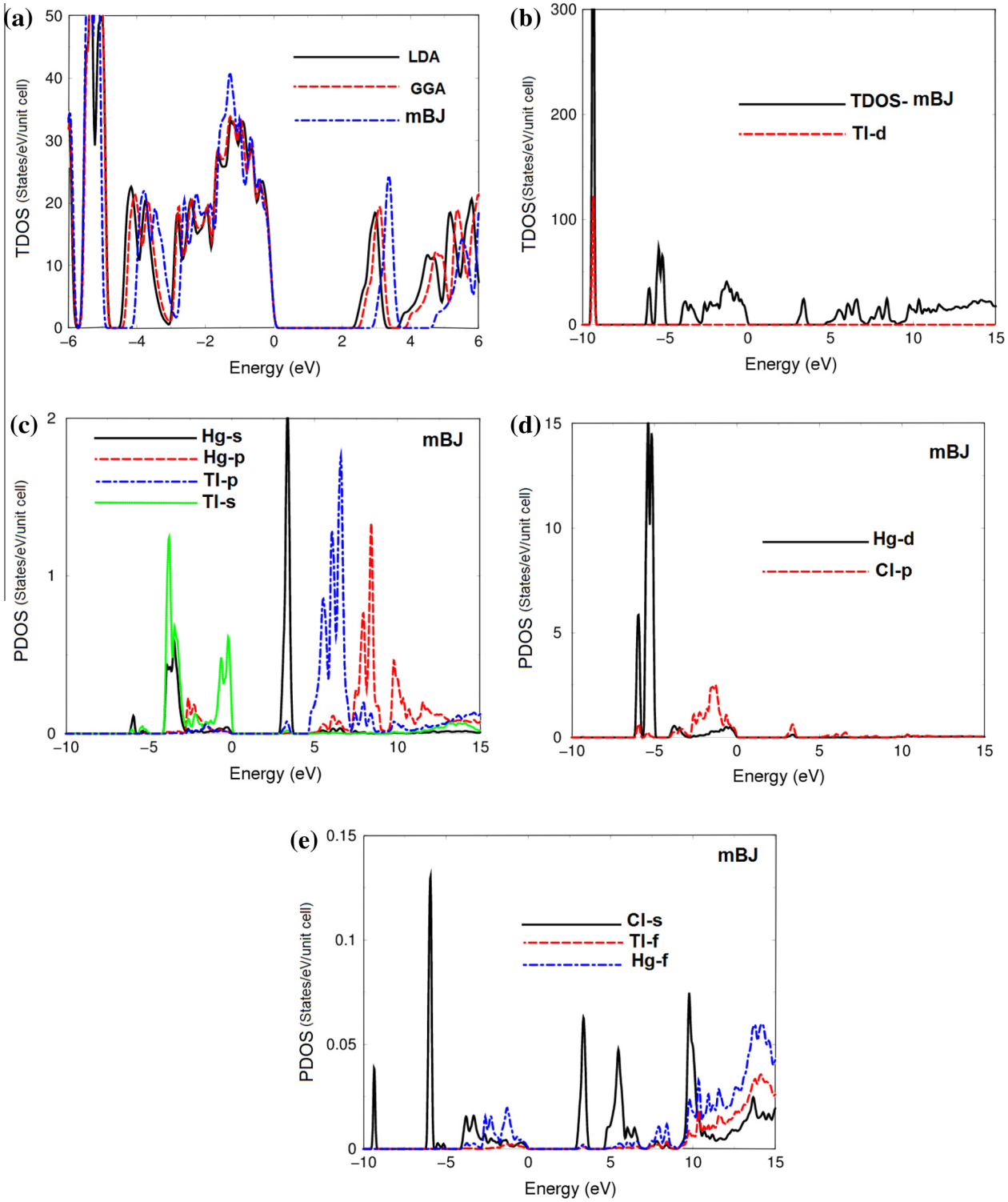

Fig. 7. Calculated partial density of states for $TlHgCl_3$ single crystal; (a) calculated total density of states using CA-LDA, PBE-GGA and mBJ; (b) calculated total density of states along Tl-d partial density of states using mBJ; (c) partial density of states for Hg-s/p and Tl-s/p states using mBJ; (d) partial density of states for Hg-d and Cl-p; (e) partial density of states for Hg-f, Tl-f and Cl-s.

interatomic distances as shown in Fig. 4 confirm the anisotropic nature of bonding in $TlHgCl_3$.

2.2.3. Linear optical response

Since $TlHgCl_3$ crystallizes in orthorhombic structure with space group *Pnma*, there are three non-zero components of the second-order dielectric (optical) tensor corresponding to the electric field $\vec{E}$ being directed along **a**, **b**, and **c**-crystallographic axes. We identify these with the Cartesian coordinates (x, y and z) corresponding to [100], [010] and [001] polarization directions. $TlHgCl_3$ single crystal possesses well pronounced structures of the three non-zero major complex tensor components, $\varepsilon^{xx}(\omega)$, $\varepsilon^{yy}(\omega)$ and $\varepsilon^{zz}(\omega)$. The imaginary part, $\varepsilon_2^{xx}(\omega)$, $\varepsilon_2^{yy}(\omega)$ and $\varepsilon_2^{zz}(\omega)$ of the optical function's dispersion completely defines the linear optical

properties, which originates from inter-band transitions between valence and conduction bands. The imaginary parts can be obtained using the expression taken from Ref. [29]:

$$\varepsilon_2^{ij}(\omega)=\frac{8\pi^2\hbar^2e^2}{m^2V}\sum_k\sum_{cv}(f_c-f_v)\frac{p^i_{cv}(k)p^j_{vc}(k)}{E^2_{vc}}\delta[E_c(k)-E_v(k)-\hbar\omega] \quad (3)$$

where m, e and $\hbar$ are the electron mass, charge and Planck's constant, respectively. f_c and f_v represent the Fermi distributions of the conduction and valence bands, respectively. The term $p^i_{cv}(k)$ denotes the momentum matrix element transition from the energy level c of the conduction band to the level v of the valence band at certain **k**-point in the BZ and V is the unit cell volume.

Fig. 9(a) exhibits the imaginary part of the optical function's dispersion. Following the calculated electronic band structure and the partial density of states we can indicate the optical transitions occurs in the major structure of, $\varepsilon_2^{xx}(\omega)$, $\varepsilon_2^{yy}(\omega)$ and $\varepsilon_2^{zz}(\omega)$. The first spectral structure (0.0–5.0 eV) of, $\varepsilon_2^{xx}(\omega)$, $\varepsilon_2^{yy}(\omega)$ and $\varepsilon_2^{zz}(\omega)$ is due to the transition from Hg-d/f, Cl-p and Tl-p states to Hg-s and Cl-s states. The second spectral structure (5.0–10.0 eV) could be explained by the optical transitions between Tl-p and Hg-s/p states to Tl-s and Hg-s states. The last structure (10.0–13.5 eV) arises by the optical transitions from Hg-s/d, Tl-p and Cl-s to Hg-p/f, Tl-s/f and Cl-s states. Fig. 9(a) shows that the first transition occurs at 2.69 eV, followed by first spectral structure. The main spectral structure is situated between 5.0 eV and 7.5 eV. The third spectral structure lies between 8.0 eV and 13.5 eV. At low energies $\varepsilon_2^{zz}(\omega)$ is the dominate component while at higher energies the three components contribute equally. There exists a considerable anisotropy between the three spectral components along the energy range. By means of Kramers–Kronig transformation [30] one can obtain the real part of the corresponding principal complex tensor components from the existing information about the imaginary part. The real part, $\varepsilon_1^{xx}(\omega)$, $\varepsilon_1^{yy}(\omega)$ and $\varepsilon_1^{zz}(\omega)$ of $TlHgCl_3$ single crystal is illustrated in Fig. 9(b), which show that the, ε_1^{xx}, ε_1^{yy} and ε_1^{zz} values are 3.35, 3.40 and 4.09, respectively.

From the existing information on the imaginary and real parts of the optical function's dispersion we can calculate the other optical properties such as reflectivity spectra $R(\omega)$ and absorption coefficient $I(\omega)$. The reflectivity spectra along [1 00], [010] and [001] polarization directions are represented in Fig. 9(c). At the low energy region (0.0–2.5 eV) both of $R^{xx}(\omega)$ and $R^{yy}(\omega)$ spectral components exhibit low reflectivity of about 9.0% whereas $R^{zz}(\omega)$ behave as the dominant component with reflectivity of about 11.0%. The reflectivity spectra of the three spectra components varies along the energy scale to reach the maximum value (60.0%) at around 13.5 eV, which results from the transitions of s-states of valence bands to p-states of conduction bands, confirming the occurrence of a collective plasmon resonance. $TlHgCl_3$ shows the first reflectivity maximum (~22.0%) at around 4.0 eV followed by the second reflectivity maximum (~44.0%) at around 6.0 eV and the first reflectivity minima situated at around 8.0 eV. The first reflectivity maximum and minimum are occur according to the transition from p-states of Cl and Tl atoms (valence bands) to s-states of Hg and Cl toms (conduction bands). Fig. 9(d) represents the calculated absorption coefficient $I(\omega)$ in comparison with our measured absorption coefficient. It is clear that both of the calculated and measured absorption coefficient shows the fundamental optical absorption edge at around 2.74 eV. After the fundamental optical absorption edge the absorption coefficient increases drastically to reach maximum value at around 13.5 eV. It is clear that the $TlHgCl_3$ single crystal exhibit a wide optical transparency region (918–4525 Å). Fig. 9(e) represents the comparison between the average of the three components of the theoretical absorption coefficient with the experimental absorption coefficient. One can see there exists reasonably good agreement between our calculated and measured absorption coefficient.

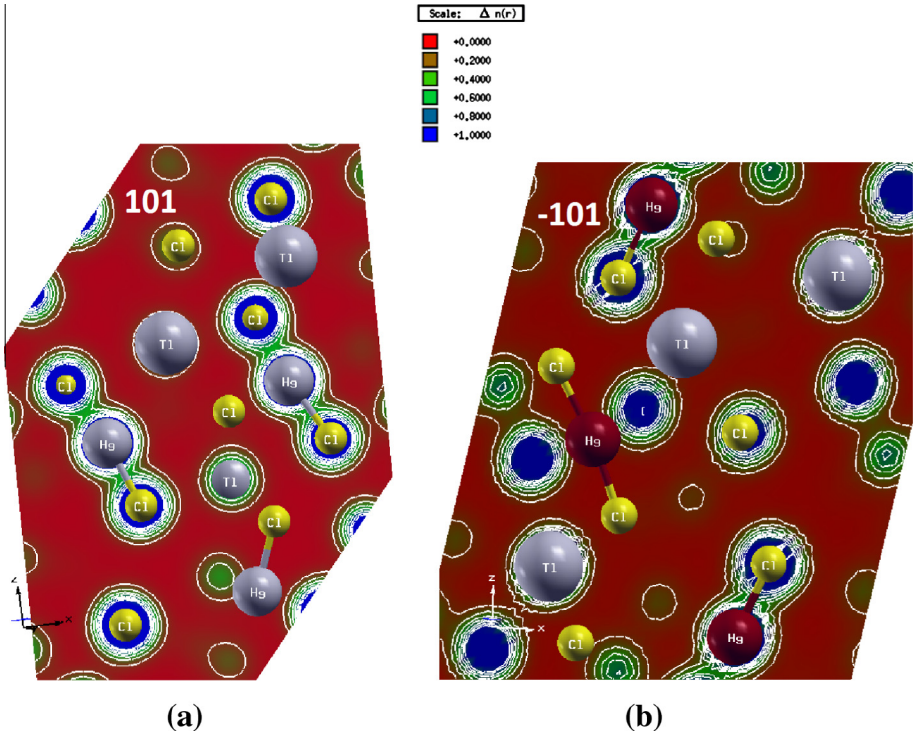

Fig. 8. Calculated electronic charge density counters using mBJ; (a) illustrated the electronic charge density contour in (1 0 1) crystallographic plane which represents all atoms; (b) illustrated the electronic charge density contour in (−1 0 1) crystallographic plane which represents all atoms.

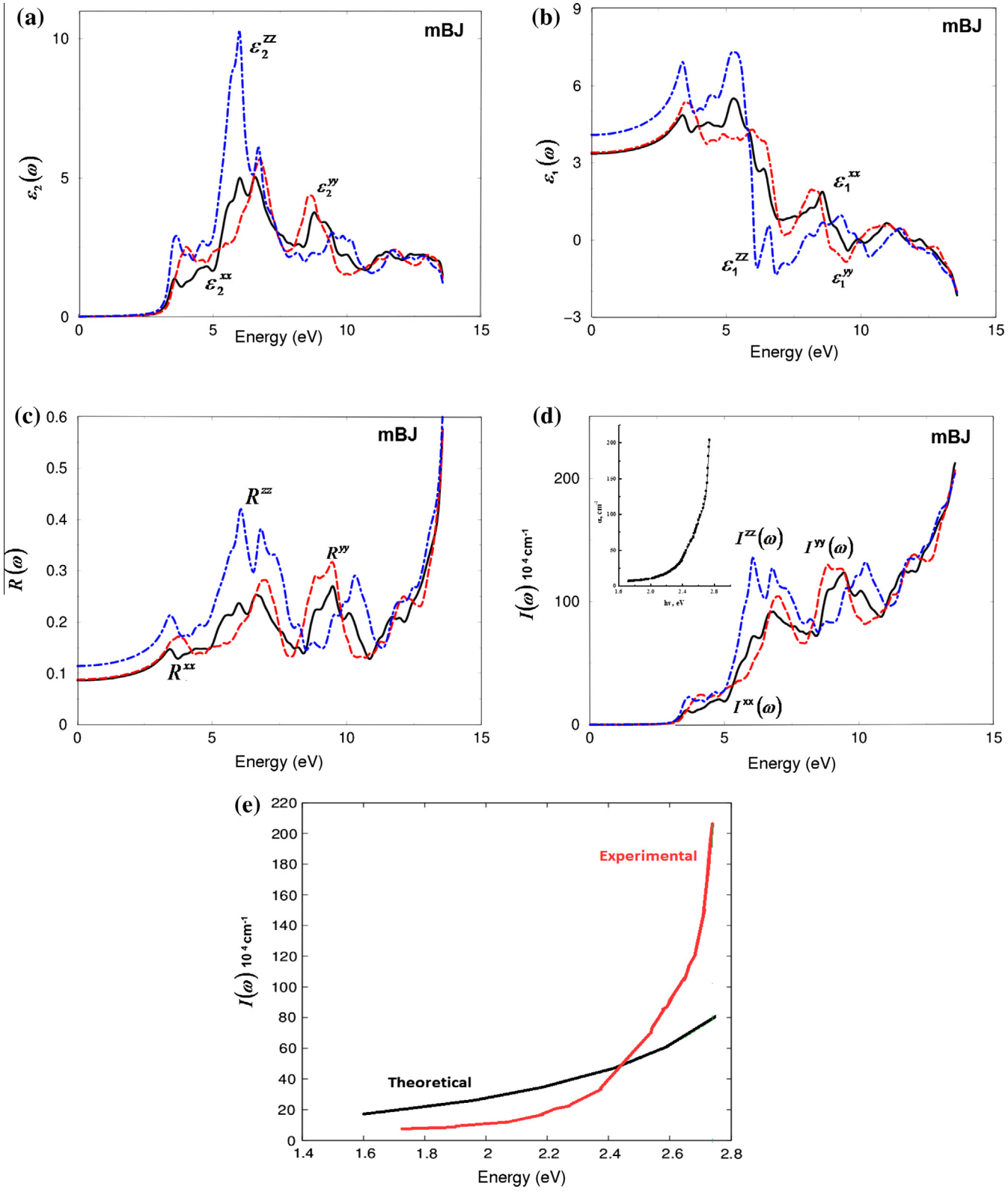

Fig. 9. (a) Calculated $\varepsilon_2^{xx}(\omega)$ (dark solid curve-black color online), $\varepsilon_2^{yy}(\omega)$ (light dashed curve-red color online) and $\varepsilon_2^{zz}(\omega)$ (light dotted dashed curve-blue color online) dispersion spectra using mBJ; (b) calculated $\varepsilon_1^{xx}(\omega)$ (dark solid curve-black color online), $\varepsilon_1^{yy}(\omega)$ (light dashed curve-red color online) and $\varepsilon_1^{zz}(\omega)$ (light dotted dashed curve-blue color online) spectra using mBJ; (c) calculated $R^{xx}(\omega)$ (dark solid curve-black color online), $R^{yy}(\omega)$ (light dashed curve-red color online), and $R^{zz}(\omega)$ (light dotted dashed curve-blue color online) using mBJ; (d) calculated absorption coefficient $I^{xx}(\omega)$ (dark solid curve-back color online), $I^{yy}(\omega)$ (light dashed curve-red color online) and $I^{zz}(\omega)$ (light dotted dashed curve-blue color online) spectrum using EV-GGA in comparison with our experimental data, the absorption coefficient in 10^4 cm^{-1}. (e) Comparison between the average of the theoretical absorption coefficient and experimental absorption coefficient. All optical properties are calculated using mBJ. (For interpretation of the references to color in this figure legend, the reader is referred to the web version of this article.)

3. Conclusions

The diffraction pattern of the $TlHgCl_3$ composition is recorded by a DRON 4-13 diffractometer with Cu Kα radiation and a Ni filter is indexed in the assumption of the orthorhombic cell with the periods $a = 9.1601(4)$ Å, $b = 4.3548(2)$ Å, $c = 14.0396(5)$ Å. An optical absorption measurement for $TlHgCl_3$ are performed on parallel-plate samples with polished optical quality surfaces of $d = 0.03$ mm. A band gap of about 2.74 eV is measured from the fundamental absorption edge at $\alpha = 200\ cm^{-1}$. As a starting point for the DFT calculation we have used our measured crystallographic data. We have optimized the geometry by minimization the forces acting on each atom using PBE-GGA within the FP-L(APW + lo) method. From the relaxed geometry we have calculated the electronic band structure, total and partial density of states, electronic charge density distribution and the optical properties using LDA, PBE-GGA and mBJ exchange correlation potentials. We find that the mBJ gives an energy band gap close to the experimental value. The calculated partial density of states helps to identify the angular momentum character of the various structures and the hybridizations between the states in order to identify the bonding nature. The interatomic distances and the two crystallographic planes (1 0 1) and (−1 0 1) confirm the anisotropic nature of bonding in $TlHgCl_3$. Further insight into the electronic structure can be obtained from the optical properties. Therefore the optical properties are measured and calculated, and good agreement is found.

Acknowledgments

The result was developed within the CENTEM project, reg. no. CZ.1.05/2.1.00/03.0088, cofunded by the ERDF as part of the Ministry of Education, Youth and Sports OP RDI programme and, in the follow-up sustainability stage, supported through CENTEM PLUS (LO1402) by financial means from the Ministry of Education, Youth and Sports under the "National Sustainability Programme I". Computational resources were provided by MetaCentrum (LM2010005) and CERIT-SC (CZ.1.05/3.2.00/08.0144) infrastructures.

SA would like to thank CSIR-NPL and Physics Department IIT Delhi for financial support.

Appendix A. Supplementary material

Supplementary data associated with this article can be found, in the online version, at http://dx.doi.org/10.1016/j.optmat.2015.06.018.

References

[1] K.S. Aleksandrov, A.T. Anystratov, B.V. Beznosykov, Akad, Avtometryya (1) (1978) 50.
[2] K. Brodersen, G. Thiele u. G. Görz, Z. Anorg. Allg. Chem. 401 (1973) 217.
[3] K. Brodersen, K.P. Jensen, D. Messer, G. Thiele, H.J. Berthold, D. Haas u. R. Tamme, Z. Anorg. Allg. Chem. 456 (1979) 29.
[4] K. Brodersen, K.P. Jensen, G. Thiele, Z. Naturforsch. 35 b (1980) 259.
[5] P. Rodnyi, Physica Processes in Inorganic Oscillators, CTC Press, 1996.
[6] M.M. Lee, J. Teuscher, T. Miyasaka, T.N. Murakami, H.J. Snaith, Science 338 (6107) (2012) 643–647.
[7] Giles E. Eperon, Samuel D. Stranks, Christopher Menelaou, Michael B. Johnston, Laura M. Herz, Henry J. Snaith, Energy Environ. Sci. 7 (3) (2014) 982.
[8] Nakita K. Noel, Samuel D. Stranks, Antonio Abate, Christian Wehrenfennig, Simone Guarnera, Amir-Abbas Haghighirad, Aditya Sadhanala, Giles E. Eperon, Sandeep K. Pathak, Michael B. Johnston, Annamaria Petrozza, Laura M. Herz, Henry J. Snaith, Energy Environ. Sci. 7 (9) (2014) 3061.
[9] Henry J. Snaith, Antonio Abate, James M. Ball, Giles E. Eperon, Tomas Leijtens, Nakita K. Noel, Jacob Tse-Wei Wang, Konrad Wojciechowski, Wei Zhang, Wei Zhang, J. Phys. Chem. Lett. 5 (9) (2014) 1511–1515.
[10] K.S. Aleksandrov, BV Beznosykov hierarchy perovskytopodobnыh krystallov, Solid State Phys. 39 (5) (1997).
[11] K. Brodersen, K.-P. Jensen, G. Thiele, Z. Naturforsch. 35b (1980) 253–258.
[12] S.V. Mel'nikova, A.T. Anistratov, B.V. Beznosikov, Optical properties of ABCl3 type crystals, Fizika Tverdogo Tela 19 (7) (1977) 2161–2164.
[13] H. Brasseur, L. Pauling, J. Am. Chem. Soc. 60 (1938) 2886.
[14] C.H. MacGillavry, H. Nijveld, S. Dierdorp, J. Karsten, Ree. Trav. Chim. Pays-Bas 58 (1939) 193.
[15] A.H. Reshak, Xuean Chen, S. Auluck, H. Kamarudin, J. Appl. Phys. 112 (2012) 053526.
[16] A.H. Reshak, M.G. Brik, S. Auluck, J. Appl. Phys. 116 (2014) 103501.
[17] A.H. Reshak, S. Auluck, J. Appl. Phys. 116 (2014) 103702.
[18] A.H. Reshak, Hongwei Huang, H. Kamarudin, S. Auluck, J. Appl. Phys. 117 (2015) 000000, http://dx.doi.org/10.1063/1.4913693.
[19] J. Huart, Bul. Soc. Franc. Miner. Crist. 89 (1966) 23–25.
[20] A.V. Bogdanova, N.P. Zaslavskaya, E.V. Sinichka, M.F. Fedyna, I.R. Mokra, S.M. Gasinets, Synthesis and crystal structure of compounds TlCdCl3 and TlCdBr3, Inorg. Mater. 29 (1993) 664–666.
[21] M.I. Kolinko, I.V. Kityk, A.S. Krochuk, Band-energy parameters and density functions of the orthorhombic TlI crystals, J. Phys. Chem. Solids (UK) 53 (10) (1992) 1315–1320.
[22] V. Subramanian, K. Seff, Mercuric chloride, a redetermination, Acta Crystallogr. B 36 (1980) 2132–2135.
[23] B.I. Shklovskii, A.L. Efros, Electronic Properties of Doped Semiconductors, Springer, Heidelberg, 1984.
[24] P. Blaha, K. Schwarz, G.K.H. Madsen, D. Kvasnicka, J. Luitz, WIEN2k, An Augmented Plane Wave Plus Local Orbitals Program for Calculating Crystal Properties, Vienna University of Technology, Austria, 2001.
[25] W. Kohn, L.J. Sham, Phys. Rev. A 140 (1965) 1133.
[26] J.P. Perdew, S. Burke, M. Ernzerhof, Phys. Rev. Lett. 77 (1996) 3865.
[27] F. Tran, P. Blaha, Phys. Rev. Lett. 102 (2009) 226401.
[28] R.I. Eglitis, Int. J. Mod. Phys. B 28 (2014) 1430009.
[29] F. Bassani, G.P. Parravicini, Electronic States and Optical Transitions in Solids, Pergamon Press Ltd., Oxford, 1975, pp. 149–154.
[30] H. Tributsch, Z. Naturforsch. A 32A (1977) 972.